

Numerical Investigation of Micro-Galvanic Corrosion in Mg Alloys: Role of the Cathodic Intermetallic Phase Size and Spatial Distributions

V. K. Beura, P. Garg, V. V. Joshi, and K. N. Solanki

Abstract

Magnesium alloys are of increasing interest in structural applications due to their low-density, moderate specific strength and stiffness, recyclability, and high damping among other properties. However, the wide-scale applicability of magnesium alloys in structural applications has been limited due to many factors including its poor corrosion resistance. In this work, a numerical investigation to simulate the micro-galvanic corrosion behavior was performed to examine the influence of the size and distribution of cathodic intermetallic phase (β -Mg₁₇Al₁₂) in a Mg matrix. The ratio of cathodic to anodic surface area was kept constant in each simulation condition to understand the effect of size and spacing distributions. In general, fragmentation of a larger intermetallic particle into smaller ones was determined to enhance the localized current density. However, the uniform distribution rather than clustered or non-uniform distribution of this small intermetallic phase throughout the matrix was found to reduce the overall dissolution current density and hence, pitting corrosion severity.

Keywords

Cathodic particles • Numerical simulation • Localized corrosion • Fragmentation

Introduction

A combination of high strength to weight ratio, excellent biocompatibility, and superior damping capacity makes magnesium (Mg) based alloys a prime material for

V. K. Beura · P. Garg · K. N. Solanki (✉)
School for Engineering of Matter, Transport and Energy,
Arizona State University, Tempe, AZ 85287, USA
e-mail: kiran.solanki@asu.edu

V. V. Joshi
Pacific Northwest National Laboratory, Energy and Environment
Directorate, 902 Battelle Boulevard, Richland, WA 99354, USA

automotive, biomedical and structural applications [1–5]. However, poor corrosion resistance of these alloys limits their widespread applicability. For instance, with Mg being the most electrochemically active element in the periodic table, Mg-based alloys undergo severe galvanic corrosion while forming joints with other structural materials [6]. In addition, Mg alloys undergo localized corrosion due to the presence of cathodic second phase particles and inclusion within the matrix [7–9]. The severity of localized corrosion is strongly dependent on the size and spacing distributions of the second phase within the Mg matrix. Besides cathodic particles, grain size [10, 11], crystal texture [12, 13] and prior processing conditions [14, 15] also alters the general corrosion behavior of Mg alloys. Therefore, suitable optimization of mentioned parameters (e.g., particle size and spacing distribution, heat treatment, etc.) can be done to tailor and improve the corrosion resistance of Mg alloys.

In most Mg alloys, Al₈Mn₅ and β -Mg₁₇Al₁₂ are the main cathodic intermetallic particles [7, 16] and their size/spacing distribution depends on different thermo-mechanical heat treatment processes. Many studies have focused on understanding the influence of change in the cathodic particle distribution on the corrosion behavior as well as mechanical properties of Mg alloys [17–21]. Fragmentation and rearrangement of β phase along with generation of different defects like vacancies, dislocation, and twins have been observed to degrade the corrosion resistance of hot-extruded AZ91 alloy with respect to its cast counterpart [15]. Similarly, the corrosion susceptibility of equal channel angular extrusion (ECAE) processed Mg alloys was found higher in comparison to as-cast pure Mg and AZ31 alloys due to its high dislocation density and smaller deformed grains [22, 23]. In contrast, Zhang et al. showed that extruded Mg alloys have enhanced corrosion resistance in comparison to as-cast Mg alloy due to grain refinement and rearrangement of second phase particles although there is an increase in dislocation and defect density with deformation [24]. This ambiguity arises from the presence and inter-dependance of a number of factors like grain size, texture, defect density

due to deformation, second phase particle size and distribution in the matrix. Therefore, it is highly important to understand the individual effect of each parameter as well as their interdependence to design future generations of Mg-based alloys.

It is difficult to deconvolute the effect of above-mentioned parameters through experimental technique performed by different thermo-mechanical processes due to their interdependence and complexity of real-time corrosion process. However, a combined approach of experiments along with simulations can be a viable approach to tackle this problem. Many studies have been performed to simulate the galvanic corrosion [25–28] and localized corrosion behavior in aluminum [29, 30] and magnesium alloys [31] and validated with the required experimental work [32]. However, a limited number of works have been performed to apply the simulation methodology to study the influence of above-described parameters on the corrosion behavior of Mg-based alloys. Taleb et al. [33] studied the effect of grain size on corrosion behavior through a simulation study using cellular automata model. Similarly, Deshpande [31] investigated the effect of β phase morphology and phase fraction on micro galvanic corrosion behavior of Mg alloys using a finite element based model. However, generally during thermo-mechanical processing in combination to phase morphology its distribution varies keeping average surface fraction constant and this variation in distribution affects the corrosion properties as observed experimentally in ECAE, extrusion, and shear assisted processing and extrusion (ShAPE) [34–36] of Mg-based alloys. Therefore, in this study, a finite element based numerical framework was used to study the effect of size and distribution of cathodic intermetallic phase (β -Mg₁₇Al₁₂) on localized corrosion behavior of Mg alloy. A single cathodic intermetallic phase was disintegrated into several smaller particles keeping the overall cathodic surface area hence cathode to anode ratio constant, to observe the effect of fragmentation on current density of the system. Additionally, spatial distribution of fragmented particles was varied by changing the radial separation distance between them to observe the effect of distribution on the localized corrosion behavior of Mg alloy.

Model Development

The micro-galvanic/localized corrosion behavior between the matrix phase (α) and the cathodic intermetallic phase (β) in Mg alloys was simulated using Comsol simulation software. The governing Nernst plank equation was solved in the electrolyte domain over the anode and cathode electrode surface in the stationary mode. Mass transfer of ionic species in the aqueous electrolyte can be described by the

contribution from diffusion, migration, and convection which can be expressed by the Nernst Plank Equation as [27]:

$$\frac{\partial c_i}{\partial t} = -D_i \nabla^2 c_i - z_i F u_i \nabla \cdot (c_i \nabla \varphi) + \nabla \cdot (c_i V) \quad (1)$$

where D_i is the diffusion coefficient, c_i is the concentration, z_i is the charge number, u_i is the mobility of different species involved in the electrochemical processes. F , and φ , are Faraday constant, and electric potential measured with respect to standard calomel electrode and electrolyte velocity (V), respectively. Nernst plank equation (Eq. 1) can be further simplified for steady-state conditions with the following assumptions (i) negligible concentration gradient due to the well-mixed electrolyte solution; (ii) the solvent is incompressible; and (iii) the electrolyte solution is electroneutral, i.e., $\sum z_i c_i = 0$ to Eq. 2.

$$\nabla^2 \varphi = 0 \quad (2)$$

Equation 2 represents the Laplace of electric potential with the upper bound of corrosion rate after neglecting the transport term due to diffusion and convection. Equation 2 was solved numerically in the electrolyte domain with appropriate boundary conditions like in the anodic and cathodic surface gradient of electrolyte potential field is directly proportional to current density, and can be written as:

$$j = -\sigma \nabla_n \varphi \quad (3)$$

where σ is the conductivity of electrolyte (2.5 S/m).

Two computational domains were used in this study to simulate the localized corrosion behavior of Mg alloy (Fig. 1). Figure 1a shows a square domain of size 50 μm \times 50 μm that represents the electrolyte over cathode (β) and anode (α) 1D electrode surface and it was used to study the effect of second phase particle size and separation on localized corrosion behavior in Sects. 3.1 and 3.2 respectively. The cylindrical domain, shown in Fig. 1b was used to study the effect of second phase particle fragmentation and distribution on localized corrosion behavior in Sect. 3.3. The cylindrical domain has base diameter of 50 μm and height of 50 μm that represents the electrolyte over cathode (β) and anode (α) 2D electrode surface. Volume and conductivity of the electrolytes in both the domains were kept constant throughout the study. However, the size of electrode surfaces was varied keeping combined electrode surface length (50 μm) and electrode surface area (1962.5 μm^2) constant in both 1D and 2D computational domains, respectively. Insulating boundary conditions were used at all boundaries of the computational domain except for the electrode surfaces where electrolyte potential was solved using Eq. 3.

Furthermore, current density evolution at cathode and anode electrode surfaces was solved using anodic and cathodic Tafel extrapolation parameters as input variables. Experimental polarization curves for alpha (α) and beta (β) were used [31] to extract the required electrochemical parameters using EC-lab software. Table 1 shows the list of electrochemical parameters used to simulate micro-galvanic corrosion behavior in Mg alloy.

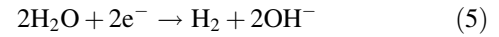
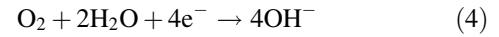
Result and Discussion

Effect of Second Phase Particle Size

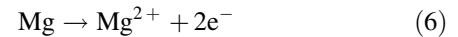
The variation in size of second phase particles in Mg alloys ranging from micrometers to nanometers is significantly dependent on the prior heat treatment and thermo-mechanical processing of the alloy [37]. Localized corrosion in Mg alloys also depends on the size of the cathodic phases beside their composition. Therefore, to understand the size effect of β phase on corrosion behavior particles of different radius ($R_{\text{particles}}$) were used to study the variation of cathodic and anodic current density in the electrochemical system. Figure 2 shows the variation of current density as a function of cathodic particle size from 2 to 10 μm . The cathodic current density increased on the β phase surface with increase in surface area of the second phase particle. Thus, the larger surface area provides more sites for cathodic reactions like hydrogen evolution and oxygen reduction (Eqs. 4 and 5) and drives the anodic reactions on the Mg matrix adjacent to the particle. The cathodic current density increased from -23.5 to -17.5 A/m^2 , around 30%, with increase of R_{particle} from 2 to 10 μm . This increase in cathodic current density enhanced anodic dissolution

reaction on Mg matrix (Eq. 6) which shows an eight-fold increase in anodic current density as R_{particle} increased from 2 to 10 μm (Fig. 2b). Thus, the region with bigger cathodic particle enhances localized matrix dissolution which makes the usage of alloy more detrimental for longer term as compared to the alloy with smaller cathodic particles.

Cathodic reaction:



Anodic reaction:



Effect of Second Phase Particle Separation

Along with second phase particle size and composition, the separation between the particles also plays a crucial role to determine the intensity of localized corrosion. This separation distance depends on several factors like mechanical deformation, heat treatment, and other thermo-mechanical processing. The separation distance controls the interaction between two cathodic particles as well as the transport of reacting species within the local electrolyte. To observe the effect of separation distance (S) two identical particles of different sizes (R_{particle}) were used to study the corrosion behavior of the common matrix present in between them. Figure 3a shows the variation in anodic current density of the common matrix as a function of the separation distance. The anodic current density of the matrix increased with

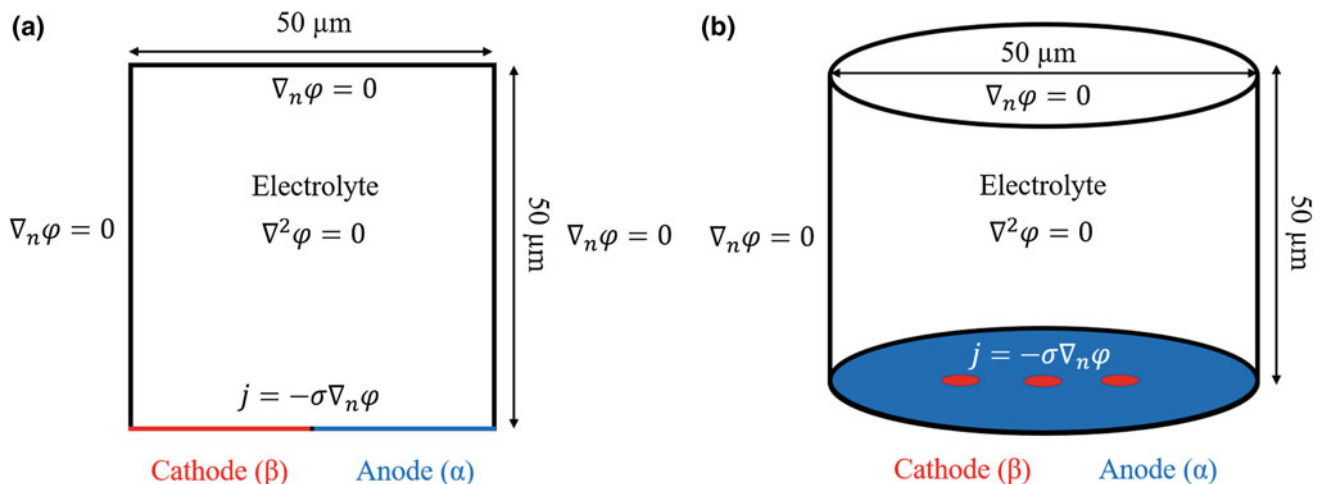
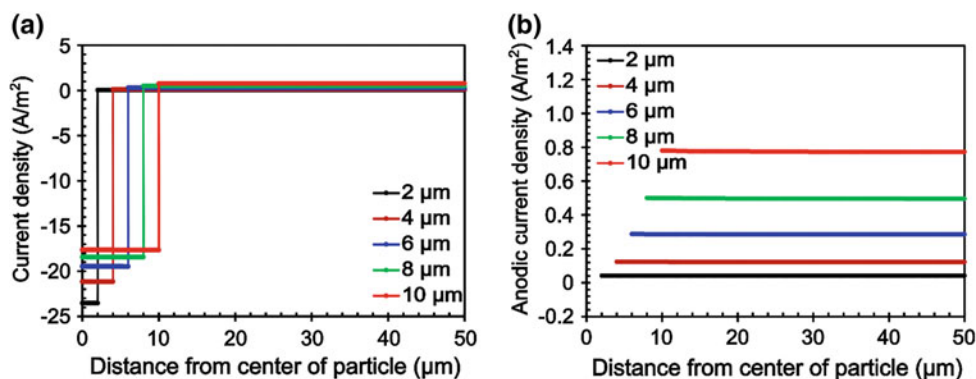


Fig. 1 Computational domain of electrochemical system with necessary equations and boundary conditions for reacting and insulating surfaces. Red and blue lines/circles, respectively represent the cathode and anode electrode a 1D and b 2D surfaces

Table 1 Electrochemical parameters used in this study to simulate the corrosion behavior of Mg alloy

Electrochemical parameters	Alpha (α)	Beta (β)
Corrosion potential (V, SCE)	-1.424	-1.151
Exchange current density (A/m^2)	0.081	0.017
Tafel slope (V/decade)	0.008	-0.0835
Electrolyte conductivity (S/m)	2.5	

Fig. 2 Effect of cathodic β phase size on the corrosion behavior a Variation in cathodic and anodic current density with β phase size (R_{particle}). b Variation in anodic current density of adjacent matrix with β phase size (R_{particle})



decreasing the separation distance between the particles which directly corresponds to the higher dissolution reaction at the matrix. As the separation distance increased further, a parabolic variation of matrix anodic current density was observed which was highest at the interface of cathodic particle and the matrix and it gradually decreased as we move away from interface showing a decrease in the inter-particle interaction. This variation of current density can be correlated with anodic and cathodic reactions on both the surfaces and their transport within the electrolyte. Due to shorter distance between particles like $0.4 \mu\text{m}$, availability of reducible species like O_2 is easier due to smaller transport distances between the anode and cathode surfaces. This enhancement in anodic current density due to separation distance varies with size of the cathodic particle shown in Fig. 3b. A fivefold increase in current density can be observed with increase in R_{particle} from 2 to $10 \mu\text{m}$.

Effect of Second Phase Particle Fragmentation and Separation

Generally, during processing and real-time applications both cast and processed Mg alloys undergo extreme conditions of high strain-rate deformation and/or high-temperature applications that lead to variation in cathodic particles distribution keeping the average area fraction constant. This process can also lead to the disintegration of larger cathodic particles into clusters of small-sized particles. Therefore, to understand the effect of such a complex process along with other microstructural changes can be a difficult task in terms of experimental characterization. Hence, a simulation study has

been implemented to understand effect of this phenomenon on corrosion behavior of Mg alloys. A cathodic β phase particle with $10 \mu\text{m}$ radius was fragmented into smaller particles keeping the overall cathodic surface area and the ratio of anode to cathode surface area constant. Hence, the radius (R) of fragmented particles decreased gradually with increasing number of fragmentations (N). Furthermore, the separation distance (S) between the fragmented particles was varied from 0.2 to $20 \mu\text{m}$ to observe the effect of separation between the particles on corrosion behavior. Figure 4 shows variation in magnitude of electrolyte current density with change in the number of fragmentations (N) and separation distance (S) between the cathodic particles.

The electrolyte current density was observed to vary from 0 to $23.7 A/m^2$ throughout the surface with a maximum in the region near to the cathodic particle (Fig. 4a). Furthermore, maximum current density around the cathodic particles found to increase as the number of fragmentation increased from $N = 1$ to 7 (Fig. 4a). The system with maximum number of fragmentations ($N = 7$) and the smallest separation distance ($S = 0.2 \mu\text{m}$) had the highest electrolyte current density at the cathodic particles (Fig. 4b). Whereas, the electrolyte current density was minimum at the cathodic particles in the same system with highest separation distance ($S = 20 \mu\text{m}$). To further understand these effects average electrolyte current density was calculated for each particle radius and corresponding all of the separation distances (Fig. 5).

Average electrolyte current density of single cathodic particle ($R = 10 \mu\text{m}$) serves as a reference point for other measurements (black horizontal line at $2.175 A/m^2$ in Fig. 5). The average electrolyte current density was found

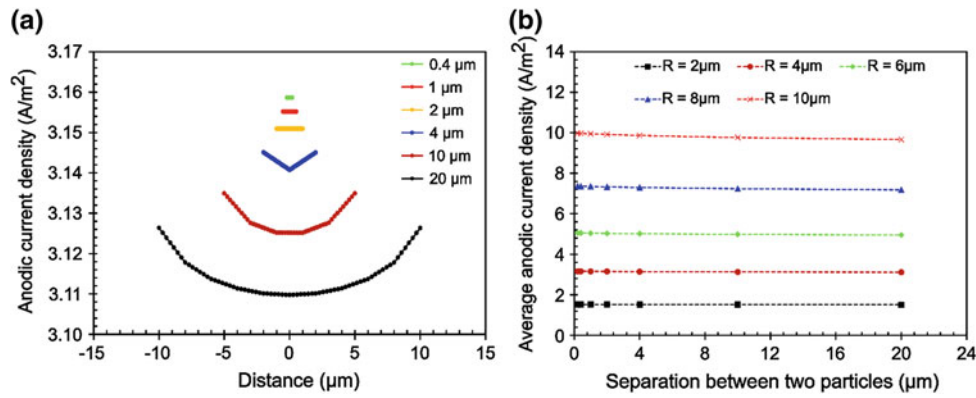


Fig. 3 Effect of cathodic β phase separation on corrosion behavior. Separation distance of zero represents the center point between two particles and +ve/-ve distances represent displacement along left/right directions, respectively. a Variation in anodic current density of matrix

between two 4 μm β phase as a function of their separation. b The average anodic current density of the matrix between two β phases as a function of phase size and separation distance

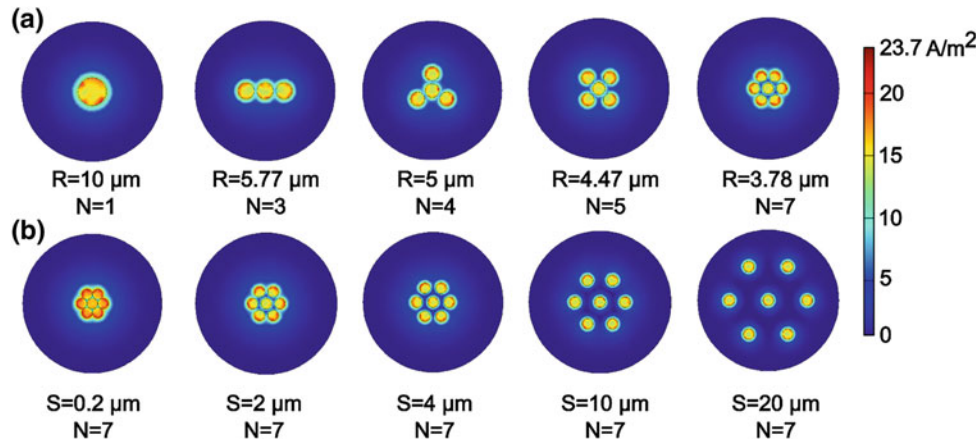


Fig. 4 Effect of cathodic particle distribution on the magnitude of electrolyte current density. a Fragmentation of single cathodic β phase into different number of particles (N) with different size (R) keeping

overall anode to cathode ratio constant. b Change in anodic current density with increasing separation distance (S) between multiple fragmentations (N = 7) of cathodic particles of same radius

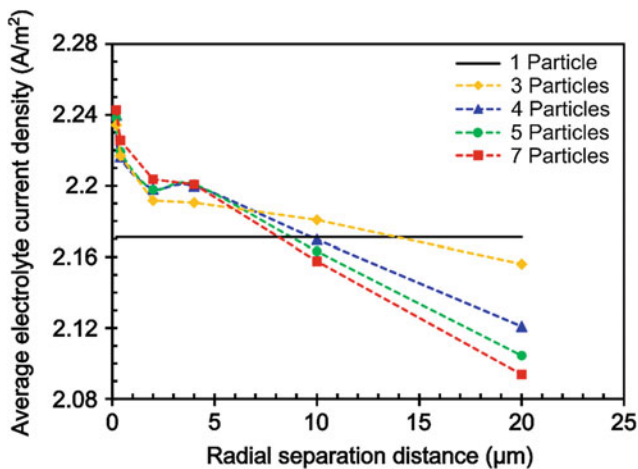


Fig. 5 Variation of average electrolyte current density with cathodic β phase fragmentations (i.e., number of particles) from a larger particle and their radial separation from the center particle

to decrease with increasing the separation distance between the particles which suggests towards a decrease in corrosion susceptibility of the alloy. These results display a similar trend observed in Fig. 3, where the anodic current density of Mg matrix decreased with the increasing separation distance between two identical cathodic particles. However, if the average electrolyte current densities for different numbers of particles were compared it shows interesting behavior. The electrochemical system with 7 particles has the highest value of average electrolyte current density than other systems (1, 3, 4, 5 particles) in the range of radial separation distance 0.2 and 4 μm . On the other hand, 7 particle system showed the lowest value of average electrolyte current density at a radial separation distance of 10 and 20 μm as compared to the other systems. Furthermore, the systems with 1, 3, 4, 5 particles showed similar behavior as the average electrolyte current density of the

system with larger number of particle systems is lower as compared to the system with lower number of particles at the radial separation distance of 10 and 20 μm . This behavior is due to decrease in the interparticle interaction and more homogenous distribution of cathodic particles with a higher number of fragmentation and radial separation. Therefore, to process a corrosion-resistant Mg alloy using various thermo-mechanical processing methods like ECAE, extrusion or ShAPE an effort should be made to have a possible smallest average particle size and the highest separation distance between the particles.

Conclusions

A comprehensive finite element based simulation study was carried out to understand the effect of size and distribution of second phase cathodic particles on localized corrosion behavior of Mg alloys. The key observations of this work are:

1. Larger cathodic particles ($R_{\text{particle}} = 10 \mu\text{m}$) enhanced anodic dissolution of the localized matrix due to enhanced cathodic reaction on their surface in comparison to the smaller size cathodic particles.
2. Interparticle interaction between two cathodic particles decreased with an increase in separation distance which reduced the anodic dissolution rate of common Mg matrix between them.
3. Corrosion behavior of Mg alloys depends on fragmentation and distribution of large cathodic particles into a cluster of smaller particles. In particular, increase in number of fragmentation enhances corrosion susceptibility of the localized system till the radial separation between the particles was less than a critical value (10 μm). However, once the separation is more than the critical value larger number of fragmentation shows the least susceptibility for corrosion.

Acknowledgements The authors would like to thank Pacific Northwest National Laboratory and the Office of Naval Research (N000141110793) for their financial assistance.

References

1. M. Esmaily, J.E. Svensson, S. Fajardo, N. Birbilis, G.S. Frankel, S. Virtanen, R. Arrabal, S. Thomas, L.G. Johansson, Fundamentals and advances in magnesium alloy corrosion, *Progress in Materials Science*. 89 (2017) 92–193. <https://doi.org/10.1016/j.pmatsci.2017.04.011>.
2. G. Song, Recent Progress in Corrosion and Protection of Magnesium Alloys, *Advanced Engineering Materials*. 7 (2005) 563–586. <https://doi.org/10.1002/adem.200500013>.
3. N.T. Kirkland, J. Lespagnol, N. Birbilis, M.P. Staiger, A survey of bio-corrosion rates of magnesium alloys, *Corrosion Science*. 52 (2010) 287–291. <https://doi.org/10.1016/j.corsci.2009.09.033>.
4. P. Garg, I. Adlakha, K.N. Solanki, Effect of solutes on ideal shear resistance and electronic properties of magnesium: A first-principles study, *Acta Materialia*. 153 (2018) 327–335. <https://doi.org/10.1016/j.actamat.2018.05.014>.
5. C. Kale, M. Rajagopalan, S. Turnage, B. Hornbuckle, K. Darling, S.N. Mathaudhu, K.N. Solanki, On the roles of stress-triaxiality and strain-rate on the deformation behavior of AZ31 magnesium alloys, *Materials Research Letters*. 6 (2018) 152–158. <https://doi.org/10.1080/21663831.2017.1417923>.
6. G. Song, B. Johannesson, S. Hapugoda, D. StJohn, Galvanic corrosion of magnesium alloy AZ91D in contact with an aluminium alloy, steel and zinc, *Corrosion Science*. 46 (2004) 955–977. [https://doi.org/10.1016/s0010-938x\(03\)00190-2](https://doi.org/10.1016/s0010-938x(03)00190-2).
7. O. Lunder, J.E. Lein, T.K. Aune, K. Nisancioglu, The Role of Mg₁₇Al₁₂ Phase in the Corrosion of Mg Alloy AZ91, *CORROSION*. 45 (1989) 741–748. <https://doi.org/10.5006/1.3585029>.
8. S. Mathieu, C. Rapin, J. Steinmetz, P. Steinmetz, A corrosion study of the main constituent phases of AZ91 magnesium alloys, *Corrosion Science*. 45 (2003) 2741–2755. [https://doi.org/10.1016/s0010-938x\(03\)00109-4](https://doi.org/10.1016/s0010-938x(03)00109-4).
9. R. Ambat, N.N. Aung, W. Zhou, Evaluation of microstructural effects on corrosion behaviour of AZ91D magnesium alloy, *Corrosion Science*. (2000) 23.
10. N.N. Aung, W. Zhou, Effect of grain size and twins on corrosion behaviour of AZ31B magnesium alloy, *Corrosion Science*. 52 (2010) 589–594. <https://doi.org/10.1016/j.corsci.2009.10.018>.
11. K.D. Ralston, N. Birbilis, Effect of Grain Size on Corrosion: A Review, *CORROSION*. 66 (2010) 075005-075005-13. <https://doi.org/10.5006/1.3462912>.
12. G.-L. Song, R. Mishra, Z. Xu, Crystallographic orientation and electrochemical activity of AZ31 Mg alloy, *Electrochemistry Communications*. 12 (2010) 1009–1012. <https://doi.org/10.1016/j.elecom.2010.05.011>.
13. Z. Pu, G.-L. Song, S. Yang, J.C. Outeiro, O.W. Dillon, D.A. Puleo, I.S. Jawahir, Grain refined and basal textured surface produced by burnishing for improved corrosion performance of AZ31B Mg alloy, *Corrosion Science*. 57 (2012) 192–201. <https://doi.org/10.1016/j.corsci.2011.12.018>.
14. H. Wang, Y. Estrin, H. Fu, G. Song, Z. Zúberová, The Effect of Pre-Processing and Grain Structure on the Bio-Corrosion and Fatigue Resistance of Magnesium Alloy AZ31, *Advanced Engineering Materials*. 9 (2007) 967–972. <https://doi.org/10.1002/adem.200700200>.
15. T. Zhang, Y. Shao, G. Meng, Z. Cui, F. Wang, Corrosion of hot extrusion AZ91 magnesium alloy: I-relation between the microstructure and corrosion behavior, *Corrosion Science*. 53 (2011) 1960–1968. <https://doi.org/10.1016/j.corsci.2011.02.015>.
16. A. Pardo, M.C. Merino, A.E. Coy, F. Viejo, R. Arrabal, S. Feliú, Influence of microstructure and composition on the corrosion behaviour of Mg/Al alloys in chloride media, *Electrochimica Acta*. 53 (2008) 7890–7902. <https://doi.org/10.1016/j.electacta.2008.06.001>.
17. S. Lee, S.H. Lee, D.H. Kim, Effect of Y, Sr, and Nd additions on the microstructure and microfracture mechanism of squeeze-cast AZ91-X magnesium alloys, *Metallurgical and Materials Transactions A*. 29 (1998) 1221–1235. <https://doi.org/10.1007/s11661-998-0249-0>.
18. D.K. Xu, W.N. Tang, L. Liu, Y.B. Xu, E.H. Han, Effect of Y concentration on the microstructure and mechanical properties of as-cast Mg–Zn–Y–Zr alloys, *Journal of Alloys and Compounds*. 432 (2007) 129–134. <https://doi.org/10.1016/j.jallcom.2006.05.123>.

19. M. Horstemeyer, High cycle fatigue of a die cast AZ91E-T4 magnesium alloy, *Acta Materialia*. 52 (2004) 1327–1336. <https://doi.org/10.1016/j.actamat.2003.11.018>.
20. H. Feng, S. Liu, Y. Du, T. Lei, R. Zeng, T. Yuan, Effect of the second phases on corrosion behavior of the Mg-Al-Zn alloys, *Journal of Alloys and Compounds*. 695 (2017) 2330–2338. <https://doi.org/10.1016/j.jallcom.2016.11.100>.
21. X. Chen, F. Pan, J. Mao, J. Wang, D. Zhang, A. Tang, J. Peng, Effect of heat treatment on strain hardening of ZK60 Mg alloy, *Materials & Design*. 32 (2011) 1526–1530. <https://doi.org/10.1016/j.matdes.2010.10.008>.
22. G.B. Hamu, D. Eliezer, L. Wagner, The relation between severe plastic deformation microstructure and corrosion behavior of AZ31 magnesium alloy, *Journal of Alloys and Compounds*. 468 (2009) 222–229. <https://doi.org/10.1016/j.jallcom.2008.01.084>.
23. D. Song, A. Ma, J. Jiang, P. Lin, D. Yang, J. Fan, Corrosion behavior of equal-channel-angular-pressed pure magnesium in NaCl aqueous solution, *Corrosion Science*. 52 (2010) 481–490. <https://doi.org/10.1016/j.corsci.2009.10.004>.
24. Z. Zhang, H. Xu, qiang Wang, Corrosion and mechanical properties of hot-extruded AZ31 magnesium alloys, *Transactions of Nonferrous Metals Society of China*. 18 (2008) s140–s144. [https://doi.org/10.1016/s1003-6326\(10\)60190-2](https://doi.org/10.1016/s1003-6326(10)60190-2).
25. I. Adlakha, B.G. Bazehhour, N.C. Muthgowda, K.N. Solanki, Effect of mechanical loading on the galvanic corrosion behavior of a magnesium-steel structural joint, *Corrosion Science*. 133 (2018) 300–309. <https://doi.org/10.1016/j.corsci.2018.01.038>.
26. K.B. Deshpande, Validated numerical modelling of galvanic corrosion for couples: Magnesium alloy (AE44)–mild steel and AE44–aluminium alloy (AA6063) in brine solution, *Corrosion Science*. 52 (2010) 3514–3522. <https://doi.org/10.1016/j.corsci.2010.06.031>.
27. B. Gholami Bazehhour, I. Adlakha, K.N. Solanki, Role of Static and Cyclic Deformation on the Corrosion Behavior of a Magnesium-Steel Structural Joint, *JOM*. 69 (2017) 2328–2334. <https://doi.org/10.1007/s11837-017-2433-4>.
28. K.A. Spies, V.V. Viswanathan, A. Soulami, Y. Hovanski, V.V. Joshi, Galvanically Graded Interface: A Computational Model for Mitigating Galvanic Corrosion Between Magnesium and Mild Steel, in: V.V. Joshi, J.B. Jordon, D. Orlov, N.R. Neelameggham (Eds.), *Magnesium Technology 2019*, Springer International Publishing, Cham, 2019: pp. 135–144. https://doi.org/10.1007/978-3-030-05789-3_21.
29. L. Yin, Y. Jin, C. Leygraf, N. Birbilis, J. Pan, Numerical Simulation of Micro-Galvanic Corrosion in Al Alloys: Effect of Geometric Factors, *Journal of The Electrochemical Society*. 164 (2017) C75–C84. <https://doi.org/10.1149/2.1221702jes>.
30. J. Xiao, S. Chaudhuri, Predictive modeling of localized corrosion: An application to aluminum alloys, *Electrochimica Acta*. 56 (2011) 5630–5641. <https://doi.org/10.1016/j.electacta.2011.04.019>.
31. K.B. Deshpande, Numerical modeling of micro-galvanic corrosion, *Electrochimica Acta*. 56 (2011) 1737–1745. <https://doi.org/10.1016/j.electacta.2010.09.044>.
32. N. Murer, R. Oltra, B. Vuillemin, O. Néel, Numerical modelling of the galvanic coupling in aluminium alloys: A discussion on the application of local probe techniques, *Corrosion Science*. 52 (2010) 130–139. <https://doi.org/10.1016/j.corsci.2009.08.051>.
33. A. Taleb, J. Stafiej, Numerical simulation of the effect of grain size on corrosion processes: Surface roughness oscillation and cluster detachment, *Corrosion Science*. 53 (2011) 2508–2513. <https://doi.org/10.1016/j.corsci.2011.04.008>.
34. J.T. Darsell, N.R. Overman, V.V. Joshi, S.A. Whalen, S.N. Mathaudhu, Shear Assisted Processing and Extrusion (ShAPE™) of AZ91E Flake: A Study of Tooling Features and Processing Effects, *Journal of Materials Engineering and Performance*. 27 (2018) 4150–4161. <https://doi.org/10.1007/s11665-018-3509-1>.
35. N.R. Overman, S.A. Whalen, M.E. Bowden, M.J. Olszta, K. Kruska, T. Clark, E.L. Stevens, J.T. Darsell, V.V. Joshi, X. Jiang, K.F. Mattlin, S.N. Mathaudhu, Homogenization and texture development in rapidly solidified AZ91E consolidated by Shear Assisted Processing and Extrusion (ShAPE), *Materials Science and Engineering: A*. 701 (2017) 56–68. <https://doi.org/10.1016/j.msea.2017.06.062>.
36. S. Whalen, N. Overman, V. Joshi, T. Varga, D. Graff, C. Lavender, Magnesium alloy ZK60 tubing made by Shear Assisted Processing and Extrusion (ShAPE), *Materials Science and Engineering: A*. 755 (2019) 278–288. <https://doi.org/10.1016/j.msea.2019.04.013>.
37. W. Fu, R. Wang, K. Wu, J. Kuang, J. Zhang, G. Liu, J. Sun, The influences of multiscale second-phase particles on strength and ductility of cast Mg alloys, *Journal of Materials Science*. 54 (2019) 2628–2647. <https://doi.org/10.1007/s10853-018-2980-2>.